EDGE ARTICLE

Check for updates

All publication charges for this article have been paid for by the Royal Society of Chemistry

Unraveling the atomic structure and dissociation of interfacial water on anatase TiO$_2$ (101) under ambient conditions with solid-state NMR spectroscopy†

Longxiao Yang‡[a] Min Huang [ID] ‡[b] Ningdong Feng,*[a] Meng Wang, [ID] [c] Jun Xu, [ID] [a] Ying Jiang, [ID] [d] Ding Ma [ID] *[c] and Feng Deng [ID] *[a]

Anatase TiO$_2$ is a widely used component in photo- and electro-catalysts for water splitting, and the (101) facet of anatase TiO$_2$ is the most commonly exposed surface. A detailed understanding of the behavior of H$_2$O on this surface could provide fundamental insights into the catalytic mechanism. This, however, is challenging due to the complexity of the interfacial environments, the high mobility of interfacial H$_2$O, and the interference from outer-layer H$_2$O. Herein, we investigate the H$_2$O/TiO$_2$ interface using advanced solid-state NMR techniques. The atomic-level structures of surface O sites, OH groups, and adsorbed H$_2$O have been revealed and the detailed interactions among them are identified on the (101) facet of anatase TiO$_2$. By following the quantitative evolution of surface O and OH sites along with H$_2$O loading, it is found that more than 40% of the adsorbed water spontaneously dissociated under ambient conditions on the TiO$_2$ surface at a loading of 0.3 mmol H$_2$O/g, due to the delicate interplay between water–surface and water–water interactions. Our study highlights the importance of understanding the atomic-level structures of H$_2$O on the surface of TiO$_2$ in catalytic reactions. Such knowledge can promote the design of more efficient catalytic systems for renewable energy production involving activation of water molecules.

Introduction

The behavior of water on the surface of metal oxide or metal is a subject of immense importance in a variety of fields such as heterogeneous catalysis, energy science, and materials science.[1–8] This is because water plays a critical role in various chemical processes that occur on the surface of these materials.[9–19] A detailed understanding of the structure and behavior of interfacial H$_2$O on these surfaces can help researchers to develop more efficient and effective catalytic systems and materials for energy storage and conversion.

One material that has been extensively studied in this regard is titanium dioxide (TiO$_2$). TiO$_2$ is widely used in various fields, including photocatalysis, solar cells, and sensors.[1–3,20–22] The surface of TiO$_2$ is highly hydrophilic, and therefore water molecules readily adsorb onto the surface. However, details of the interaction of water with the surface, the reactivity of the TiO$_2$ surface, the rupture of the water O–H bond and consequently the formation of the water–oxide interface structure are essential for the understanding of the interfacial water behavior on the TiO$_2$ surface.

A number of studies have been conducted to investigate the behavior of water on the TiO$_2$ surface. By using scanning tunneling microscopy (STM), it was reported that water molecules form a highly ordered structure on the TiO$_2$ surface, and depending on the conditions, one/two/three-dimensional water structures (monomer, dimer, trimer, tetramer, chains, and networks) could be formed on the surface.[23–27] In other reports, it was suggested that a water molecule could react with the oxygen vacancy/defect or rupture over the low coordination surface Ti sites of TiO$_2$, and forms two hydroxyls.[11,28–31] Very recently, by an elegant environmental TEM method, Wang *et al.* reported that the four-coordinated Ti on a (1 × 4) reconstructed

[a]State Key Laboratory of Magnetic Resonance and Atomic and Molecular Physics, National Center for Magnetic Resonance in Wuhan, Wuhan Institute of Physics and Mathematics, Innovation Academy for Precision Measurement Science and Technology, Chinese Academy of Sciences, University of Chinese Academy of Sciences, Wuhan 430071, Beijing 100049, P. R. China. E-mail: ningdong.feng@wipm.ac.cn; dengf@wipm.ac.cn

[b]School of Physics, Hubei University, Wuhan 430062, P. R. China

[c]Beijing National Laboratory for Molecular Sciences, New Cornerstone Science Laboratory, College of Chemistry and Molecular Engineering, Peking University, Beijing, China. E-mail: dma@pku.edu.cn

[d]International Center for Quantum Materials, School of Physics, Peking University, Beijing, P. R. China

† Electronic supplementary information (ESI) available. See DOI: https://doi.org/10.1039/d4sc02768j

‡ These authors contributed equally to this work.

TiO_2 (001) surface is highly active for water activation.[32] However, water adsorption and dissociation on non-defect TiO_2 has been disputed for decades.[33–36] For the interfacial H_2O on the (101) facet of anatase TiO_2, a number of theoretical calculations[37–40] and some experimental studies, including temperature-programmed desorption (TPD)[41] and STM,[23] have concluded an intact molecular adsorption of H_2O on the TiO_2 surface. In contrast, a partial dissociation of H_2O has been inferred through the observation of hydroxyls formed on the TiO_2 surface by using spectroscopic techniques, such as X-ray diffraction (XRD), X-ray photoelectron spectroscopy (XPS), sum frequency generation (SFG) and so on.[42–49] However, it is challenging to distinguish the OH groups formed by H_2O dissociation on the non-defect TiO_2 surface from either the OH groups generated by H_2O reaction with defect sites or the original OH groups present on TiO_2. Therefore, while progress has been made, the atomic-level structures of interfacial H_2O and especially its detailed interaction with the TiO_2 surface are still to be resolved. Significantly, several challenges need to be addressed[50] to get the atomic-level structures of the interplay, including how to reveal the interaction of surface oxygen and titanium atoms with interfacial H_2O, how the water splitting and hydroxyl formation occur, and the quantitative evolution of these surface oxygen species at the water/TiO_2 interface during the hydration process. All these problems are difficult to solve under working reaction conditions due to the interference from outer-layer H_2O, the high mobility of interfacial H_2O, and the complexity of interfacial environments.[15,51,52]

^{17}O NMR has long been a powerful and attractive approach for characterizing the atomic-level structure of various oxygen-containing materials due to the wide [17]O chemical shift range.[53–63] For nano-oxides, the relatively low gyromagnetic ratio, low [17]O abundance (0.037%), quadrupolar nature, and especially low proportion of surface oxygen atoms lead to a great challenge to investigate the detailed structure of surface oxygen atoms. The sensitivity and resolution were still limited despite [17]O isotopic enrichment. Recently, Peng and Grey et al. selectively enriched surface oxygen atoms on metal oxides (including CeO_2, TiO_2, and ZnO) with H_2[17]O, and distinguished surface O/OH sites from bulk oxygen by using one-dimensional (1D) ^{17}O MAS NMR spectra combined with DFT calculations.[64–66] We identified surface OH groups and (sub-)surface O sites on γ-Al_2O_3 by using the 2D proton-detected [1]H–[17]O heteronuclear correlation technique to improve the sensitivity and resolution of ^{17}O NMR spectra,[67] which would make it possible to study interactions between interfacial H_2O and oxide surfaces. To date, the detailed structures of the surface O/OH sites and their interactions with interfacial H_2O are still ambiguous, let alone quantitative evolution of the structure of these surface O/OH sites in the presence of interfacial H_2O, which should be the key to understand the H_2O–oxide interaction.

In this study, we choose anatase TiO_2 nanoparticles as the oxide model owing to their wide practical application in photo- and photoelectro-catalysis, on which the most frequently exposed surface is the (101) facet with the lowest energy, and investigated the ability of anatase (101) facet-dominated TiO_2 nanoparticles to adsorb and activate water on their surface. By using the 2D [17]O MQMAS and ^{1}H{^{17}O} J-HMQC NMR methods and other techniques, we examined the atomic-level structures of interfacial water and surface O/OH sites of TiO_2 at different water loading levels, as well as the through-bond interactions between them. Our findings show that due to the delicate interplay between water–surface and water–water interactions, the O–H bond of the adsorbed water is broken through the joint effort of coordination-unsaturated Ti_{5C} and the adjacent surface O_{2C} sites, resulting in a terminal OH group (Ti_{5C}–OH) and a proton accommodated on the surface O_{2C} site to form a bridging hydroxyl ($O_{2C}H$). By following the quantitative evolution of surface O and OH sites along with H_2O loading, it is demonstrated that at a loading of 0.3 mmol H_2O g^{-1}, over 40% of the adsorbed water was dissociated spontaneously on the TiO_2 surface. The understanding over the structure and behavior of interfacial H_2O is helpful for developing more efficient and effective catalytic systems for energy storage and conversion.

Results and discussion

Interaction of surface oxygen sites with H_2O on the (101) facet of TiO_2

Anatase TiO_2 (Fig. S1–S4 in ESI†) with predominantly (101) facets (95% percent) has been synthesized. [68,69] No oxygen vacancies were detected at liquid nitrogen temperature by the ESR spectra (Fig. S5†) before and after dehydration of the TiO_2 sample at 160 °C. The morphology of the (101) facet of anatase is well-documented.[23] It features a saw-tooth-like shape, and its top layer is composed of two coordination-unsaturated species in close proximity: the five-coordinated Ti (Ti_{5C}) and two-coordinated surface O (O_{2C}) atoms, as illustrated in Fig. 1a.

To investigate the surface sites on the (101) facet of TiO_2 that interact with H_2O, one-dimensional (1D) and two-dimensional (2D) ^{17}O MAS NMR experiments were performed on [17]O-enriched TiO_2 (with the surface layer of TiO_2 enriched with [17]O, see methods for details) with different H_2[17]O loadings. As shown in Fig. 1b, the resonances at 600–800 ppm in the ^{17}O MAS NMR spectrum of bare TiO_2 were observed, the chemical shift of which is well above the three-coordinated oxygen in the bulk (around 400–600 ppm, Fig. S6†).[65] The signal shows a broad second-order quadrupolar interaction lineshape (11.7 T), with its line width sharply decreasing with the increase of magnetic field (18.7 T, Fig. 1c). We assign the resonance to a surface O_{2C} site without interaction with H_2O on bare TiO_2, marked as O_I. Upon loading 0.03 mmol H_2[17]O over 100 mg TiO_2 (0.3 mmol g^{-1}), the shape of the signal at 600–800 ppm changes significantly, with a tip appearing at 700 ppm (Fig. 1b). At the same time, two new resonances centered at 0 and 150 ppm emerge. To gain insight into the structure of the surface oxygen sites interacting with H_2O, we used the 2D ^{17}O 3Q MAS NMR technique to remove the quadrupolar broadening and enhance the spectral resolution. For TiO_2 loaded with 0.3 mmol g^{-1} H_2[17]O, clearly, the 2D 3Q MAS spectrum resolved the overlapped resonances in the ^{17}O MAS NMR spectrum (Fig. S7†), revealing two new two-coordinated O_{2C} sites (O_{II} and O_{III}). However, the large quadrupolar interaction of the O_I site made it hardly
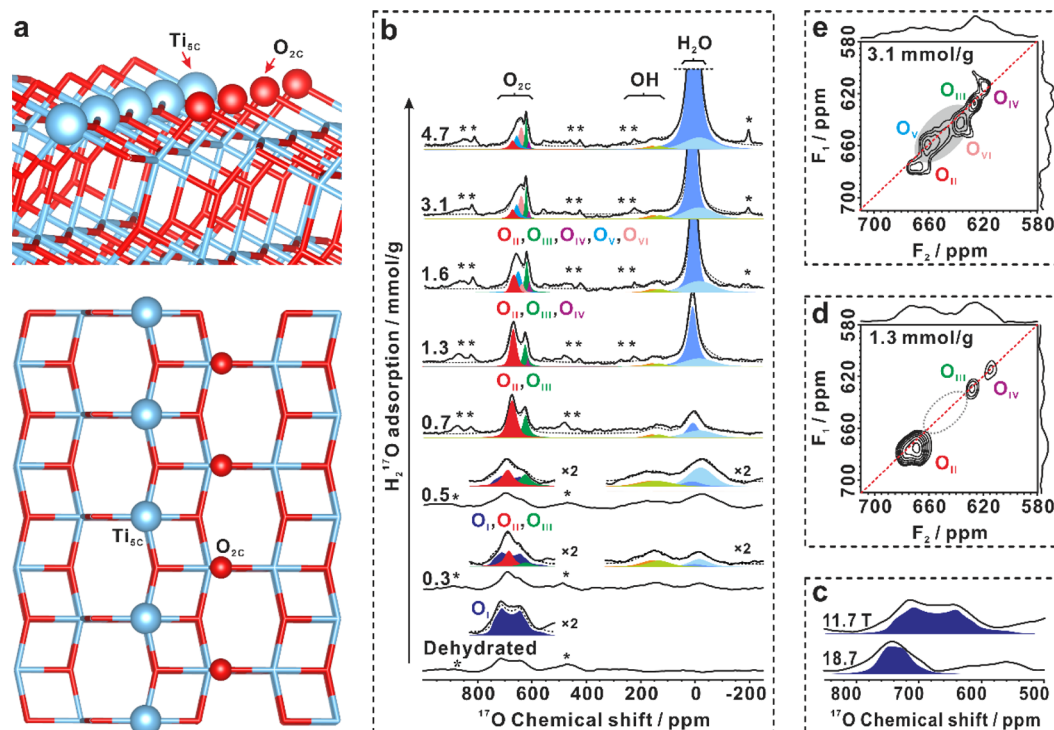
Fig. 1 Surface O_{2C} sites interacting with H_2O. (a) Ball-and-stick model of the anatase TiO_2 (101) surface with five-coordinated Ti (Ti_{5C}) and two-coordinated surface O (O_{2C}) atoms. Titanium and oxygen atoms are plotted in blue (Ti) and red (O). (b) 1D ^{17}O MAS NMR spectra of dehydrated ^{17}O-enriched TiO_2 samples with $H_2^{17}O$ loading from 0 to 4.7 mmol g^{-1}, acquired at a magnetic field of 11.7 T. Note that six O_{2C} sites (O_I–O_{VI}), two types of OH groups, and two types of adsorbed H_2O correspond to different ^{17}O peaks marked by different colors. (c) 1D ^{17}O MAS NMR spectra of ^{17}O-enriched bare TiO_2, acquired at magnetic fields of 18.7 and 11.7 T. (d-e) 2D ^{17}O 3Q MAS NMR spectra of dehydrated ^{17}O-enriched TiO_2 samples with 1.3 (d) and 3.1 mmol g^{-1} (e) $H_2^{17}O$ loading, acquired at a magnetic field of 11.7 T. Asterisks denote spinning sidebands.

observable in the 2D 3Q MAS spectrum. When the $H_2^{17}O$ loading increased to 1.3 mmol g^{-1} and then to 3.1 mmol g^{-1}, up to five signals were identified, representing five types of O_{2C} sites (O_{II}, O_{III}, O_{IV}, O_V, and O_{VI}) (Fig. 1d and e). The appearance of new O_{2C} sites at the expense of O_I sites demonstrates that a fraction of two-coordinated surface oxygen sites can interact with water molecules, leading to changes in their coordination environments.

The NMR parameters of these O_{2C} sites (O_I–O_{VI}) obtained from 1D and 2D ^{17}O 3Q MAS NMR spectra (Table S1†) were used to deconvolute the 1D ^{17}O MAS NMR signals acquired at 11.7 T and 18.7 T (Fig. 1b and S8†). The different oxygen species (O_{II}–O_{VI}) obtained upon water loading indicate different interplays between the O_{2c} sites and water. Notably, the ^{17}O MAS NMR spectrum of bare TiO_2 does not exhibit any signals of adsorbed H_2O or surface OH groups (usually at −200 to 200 ppm) (Fig. 1b). At a water loading of 0.3 mmol g^{-1}, besides the change in O_{2C} sites, the adsorbed H_2O at −50–10 ppm and two new overlapped species of surface hydroxyls at around 150 ppm emerge (Fig. 1b), which can be well resolved by the following 2D $^1H\{^{17}O\}$ J-HMQC NMR experiments. The appearance of hydroxyls suggests that water splitting occurs, which is also confirmed by ^2H MAS NMR (see the following). These results demonstrate that: (1) water can interact with the surface O_{2C} site, resulting in a change in its chemical environment, although the type and strength of the interaction cannot be

determined at the present time; and (2), ^{17}O MAS NMR experiments confirm the formation of hydroxyls arising from the dissociation of water on the TiO_2 surface.

Detailed interaction of surface oxygen/hydroxyl sites with interfacial H_2O

To better understand the structure of the interfacial scenario during water adsorption, a series of 2D $^1H\{^{17}O\}$ J-HMQC NMR experiments were conducted. These experiments allowed for the identification of ^1H–^{17}O correlation/connectivity through chemical bonds and strong hydrogen bonds. There are three types of ^1H NMR signals at 1.7, 5.4, and 7.0 ppm, which can be assigned to the proton of terminal hydroxyl, adsorbed H_2O, and bridging hydroxyl, respectively.[13,14] At $H_2^{17}O$ loadings of 0.5, 1.3 and 3.1 mmol g^{-1}, the result showed that O_{2C} sites were strongly correlated with adsorbed H_2O (5.4 ppm, Fig. S9†), indicating that the surface coordination-unsaturated O_{2C} sites were responsible for the interaction with water. Interestingly, no correlation was observed between the O_{2C} sites and terminal/bridging hydroxyls, indicating that the hydrogen in surface hydroxyls is not connected to the adjacent O_{2C} site via hydrogen-bonds.

The spatial relationship between the adsorbed water and the two surface hydroxyls was also investigated. Fig. 2a and b display the ^1H–^{17}O correlations between adsorbed H_2O and
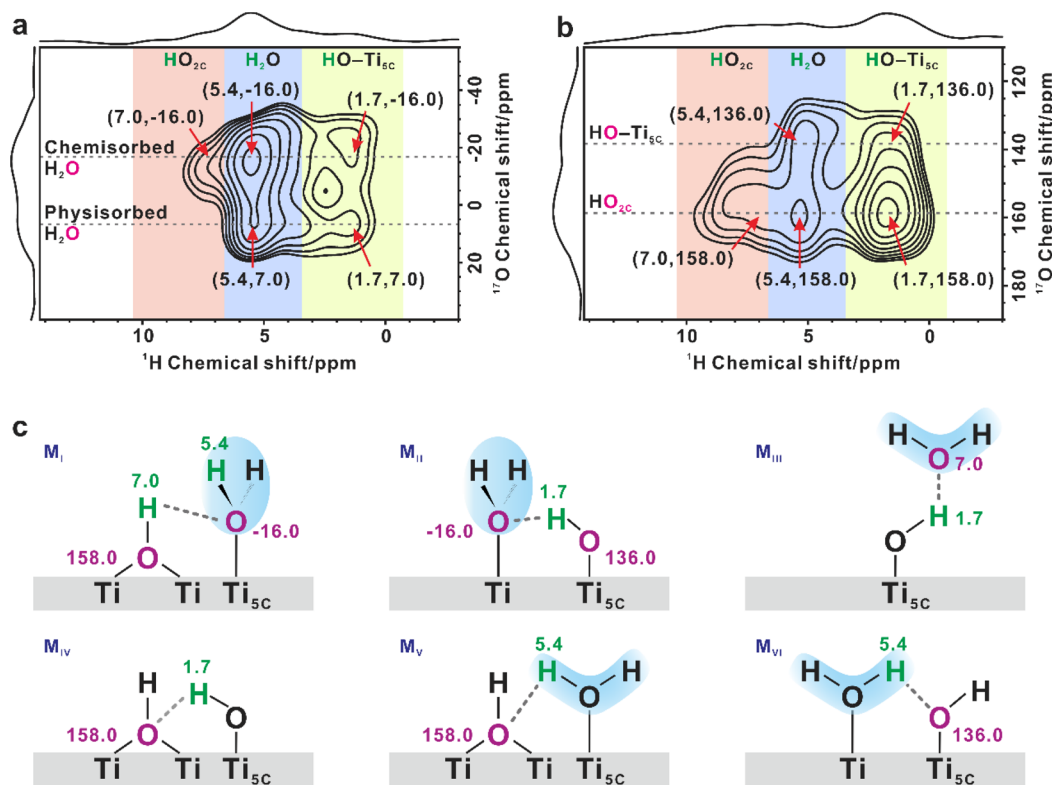
Fig. 2 Detailed structure of interfacial H_2O and OH groups on TiO_2. (a and b) 2D $^1H\{^{17}O\}$ J-HMQC NMR spectra of the dehydrated ^{17}O-enriched TiO_2 sample with 0.5 mmol g^{-1} $H_2^{17}O$ loading in different ^{17}O chemical shift ranges. (c) The schematic illustration of the different structures (M_I–M_{VI}) of surface hydroxyls and adsorbed H_2O molecules over the surface of TiO_2, with the ^1H and ^{17}O chemical shift values marked. Water molecule is shadowed in blue.

surface OH groups on TiO_2 with a 0.5 mmol g^{-1} $H_2^{17}O$ loading in different ^{17}O chemical shift ranges. As shown in Fig. 2a, two cross peaks were visible at (5.4, −16) ppm and (5.4, 7.0) ppm in the correlation experiment, indicating the presence of two types of adsorbed H_2O on the TiO_2 surface. These were ascribed to chemisorbed and physisorbed H_2O, respectively, which was validated by variable-temperature ^2H static NMR experiments (Fig. S10†). In the 1D ^{17}O MAS NMR spectra (Fig. 1b), when the H_2O loading increases from 0.3 to 4.7 mmol g^{-1}, the ^{17}O signal of adsorbed H_2O gradually narrows and shifts from −16.0 to 7.0 ppm, suggesting that the H_2O molecule is preferentially adsorbed on the unsaturated Ti_{5C} site to form chemisorbed H_2O (Ti_{5C}–OH_2, ^{17}O signal at −16 ppm), while excess H_2O molecules adsorb on the outer layer of chemisorbed H_2O and hydroxyls through hydrogen bonds to form physisorbed H_2O (^{17}O signal at 7.0 ppm).

Interestingly, the ^1H signal (7.0 ppm) of bridging hydroxyl (HO_{2C}) only correlates with the ^{17}O signal of chemisorbed H_2O (−16.0 ppm; with the most possible structure illustrated in Fig. 2c M_I), while the ^1H signal (1.7 ppm) of the terminal hydroxyl (Ti_{5C}–OH) correlates with the ^{17}O signals of both chemisorbed (Fig. 2c M_{II}) and physisorbed H_2O (7.0 ppm, Fig. 2c M_{III}). At the same time, as shown in Fig. 2b, there are two types of oxygen of hydroxyls present at 136 and 158 ppm, respectively. The ^1H (7.0 ppm) signal of HO_{2C} is only correlated with the ^{17}O signal at 158 ppm. As such, we assigned the cross

peak at (7.0, 158) ppm to the ^1H–^{17}O correlation from HO_{2C}, and ascribed the cross peak at (1.7, 136) ppm to the Ti_{5C}–OH correlation. The cross peak at (1.7, 158) ppm represents the correlation between them (Fig. 2c M_{IV}). It is worth noting that the ^1H signal of adsorbed H_2O (5.4 ppm) correlates with the ^{17}O signals of both bridging OH (158 ppm, Fig. 2c M_V) and terminal OH groups (136 ppm, Fig. 2c M_{VI}), leading to two cross peaks at (5.4, 158) and (5.4, 136) ppm. As the H_2O loading increases to 1.3 mmol g^{-1}, the cross peaks become more prominent, but the interplay remains the same (Fig. S11†).

These results indicate that water splitting is easy to happen under ambient conditions over the practical TiO_2 sample under conditions close to the working catalytic conditions, and more importantly, the interplay mode between the physisorbed or chemisorbed H_2O and the different types of hydroxyls is very complicated (Fig. 2c M_I to M_{VI}), but it could be well resolved by NMR methods. However, questions remain to answer are, how the O–H bond of water ruptured over the TiO_2 surface and whether the vacancy gets involved.

Quantitative evolution of surface oxygen/hydroxyl sites at the water/TiO_2 interface during the hydration process

To answer the questions, quantitative information about different sites and species during water adsorption was estimated from 1D ^{17}O MAS NMR spectra (Fig. 3a). As shown in Fig. 3a, the only surface O_{2C} site present on the bare TiO_2
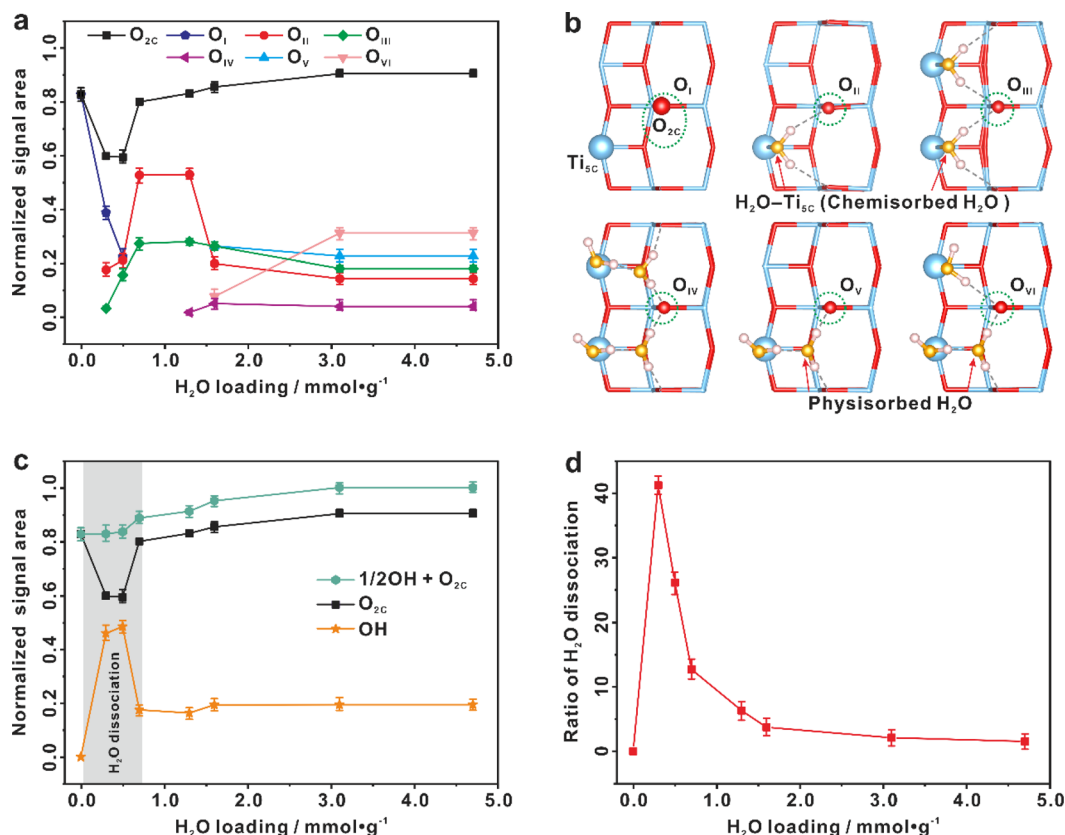
Fig. 3 Spontaneous dissociation of interfacial H_2O on the (101) facet of TiO_2 (100 mg) at room temperature. (a) Quantitative evolution of various surface two-coordinated oxygen sites (O_{2C}, including O_I–O_{VI}) with the increase of H_2O loading. (b) The possible configurations of six O_{2C} sites (O_I, O_{II}, O_{III}, O_{IV}, O_V, and O_{VI}) on the (101) facet of TiO_2 optimized from theoretically calculations. (c) Quantitative evolution of surface O_{2C} sites and hydroxyls with the increase of H_2O loading. (d) The proportion of H_2O dissociation with the increase of H_2O loading. Quantification of the O_{2C}/OH sites is conducted by fitting the main peaks and their spinning sidebands in the 1D ^{17}O MAS NMR spectra (Fig. 1b). Error bars in a, c, and d represent s.d. for each data point (three independent experiments), and points are the average values.

sample is O_I. When the H_2O loading is 0.3–0.5 mmol g^{-1}, two new O_{2C} sites (O_{II}, O_{III}) appear at the expense of the O_I site. When the H_2O loading grows up to 0.7 mmol g^{-1}, the O_{II} and O_{III} sites reach maximum, while the O_I site disappears completely. As shown in Fig. 1b, the chemisorbed H_2O (Ti_{5C}–OH_2) is predominant in the H_2O loading range of 0–0.7 mmol g^{-1}. Therefore, the O_{II} and O_{III} structures should originate from the O_I site interacting with chemisorbed H_2O. With further increasing the H_2O loading to 1.3 and then to 1.6 mmol g^{-1}, the adsorbed H_2O exists mainly in the form of physisorbed H_2O (those without direct bonding with Ti sites), and meanwhile new O_{2C} sites (O_{IV}, O_V, O_{VI}) appear (Fig. 3a). In addition, the amount of O_{II} and O_{III} sites remains almost unchanged, implying that the physisorbed H_2O molecules are mainly adsorbed on the outer-layer of chemisorbed H_2O and OH groups rather than the surface O_{2C} site. When the H_2O loading is increased to 3.1 mmol g^{-1}, the O_{VI} site increases remarkably at the expense of O_{II}, O_{III}, and O_V sites, indicating the further evolution of surface O_{2C} sites interacting with the additional physisorbed H_2O. The relative content of the O_I–O_{VI} sites eventually remains unchanged even when the H_2O loading is further increased to 4.7 mmol g^{-1}. With the above information,

we constructed six O_{2C} sites with possible H_2O adsorption patterns (Fig. 3b), which are derived from a series of calculated structures with different H_2O adsorption configurations on (2 × 2) surface slabs (Fig. S12–S24†). Obviously, the calculated ^{17}O NMR chemical shifts of these O_{2C} sites just correspond to experimental observation (Fig. S25†).

The sum of O_{2c} (O_{2C}＝O_I + O_{II} + O_{III} + O_{IV} + O_V + O_{VI}) sites shows quantitative information about the surface O_{2C} sites (Fig. 3a and c). It is relatively constant except at the water loading of 0.3–0.5 mmol g^{-1}, where the total content of surface O_{2C} sites is decreased by *ca.* 20% (see the grey region highlighted in Fig. 3c). Very interestingly, this is just the time for the appearance of OH groups whose content is increased by *ca.* 40% (Fig. 3c). This, together with the above results (Fig. 2), shows that the chemisorbed H_2O molecule on the Ti_{5C} site (H_2O–Ti_{5C}) is apt to dissociate into a terminal OH group (Ti_{5C}–OH) and a proton (H^+), and the latter protonates an adjacent surface O_{2C} site to form a bridging OH group (HO_{2C}), which "consumes" an adjacent O_{2C} site (see below Fig. 4). The proportion of water dissociation relative to total water loaded was also calculated, as depicted in Fig. 3d. Intriguingly, the highest proportion of H_2O dissociation, at 41.2%, was found at a water loading of 0.3 mmol
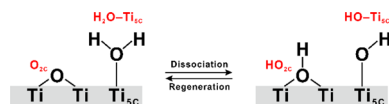
Fig. 4 Schematic diagram of H_2O dissociation and regeneration on the TiO_2 surface.

g^{-1}. With increasing the H_2O loading from 0.5 to 4.7 mmol g^{-1}, the content of surface O_{2C} sites gradually recovered and that of the hydroxyls decreased (Fig. 3c), The results point to the reaction of HO_{2C} groups with nearby Ti_{5C}–OH groups, leading to the regeneration of H_2O–Ti_{5C} and the recovery of surface O_{2C} sites. The schematic diagram of H_2O dissociation and regeneration on the TiO_2 surface is illustrated in Fig. 4.

The dissociation process of interfacial H_2O could be also confirmed by 1D ^2H MAS NMR experiments on the TiO_2 samples (Fig. 5 and S26†). The dehydrated ^2H-enriched TiO_2 was prepared by exchanging TiO_2 with 4.7 mmol g^{-1} of ^2H_2O at room temperature for 2 h, and then the ^2H-enriched sample was dehydrated at 160 °C and then loaded with different amounts (0.3–4.7 mmol g^{-1}) of ^2H_2O at room temperature. Since the proton of the bridging OH group is readily exchanged with ^2H of D_2O, only the ^2H signal of the deuterated bridging OH group (DO_{2C}) is observable at 7.4 ppm in the 1D spectrum of dehydrated TiO_2 (Fig. 5a). When 0.3 mmol g^{-1} D_2O is adsorbed on the deuterated TiO_2, in addition to the increase of the deuterated bridging OH group, a new signal at 1.6 ppm due to the deuterated terminal OH group (Ti_{5C}-OD) appears, which originates from the dissociation of D_2O (Fig. 5a). The broad signal at 4.4 ppm corresponds to adsorbed D_2O. With the increase of D_2O loading, there is a similar evolution trend for the DO_{2C} and Ti_{5C}-OD groups, especially their signal increment is roughly equal (Fig. 5b), consistent with the theoretical content ratio (1 : 1) of the two types of deuterated hydroxyls originating from the D_2O dissociation. As shown in Fig. 5b, the content of DO_{2C} and Ti_{5C}-OD groups on the TiO_2 surface reaches maximum at a 0.5 mmol g^{-1} H_2O loading, in line with the result of 1D ^{17}O MAS NMR analysis (Fig. 3c).

Theoretical insight into the adsorption and dissociation of interfacial H_2O

Based on our NMR results, a series of structures with different H_2O adsorption configurations on (2 × 2) surface slabs are optimized (Fig. S12–S24†) by density functional theory (DFT) calculations. From the adsorption energy points of view, it can be found that when the same amount of H_2O is adsorbed onto the TiO_2 (101) (2 × 2) surface slabs, the more the chemisorbed H_2O (Ti_{5C}–OH_2), the greater the adsorption energy of H_2O will be released (Table S2†), indicating that H_2O is preferentially chemisorbed on the Ti_{5C} site, forming Ti_{5C}–OH_2, and then excess H_2O is physisorbed on the Ti_{5C}–OH_2 site through the hydrogen bond, consistent with our NMR experimental results. Thus, with the increase of H_2O loading, the constructed $1H_2O/1Ti_{5C}$, $2H_2O/2Ti_{5C}$, $3H_2O/3Ti_{5C}$, $4H_2O/4Ti_{5C}$, $5H_2O/4Ti_{5C}$, $6H_2O/4Ti_{5C}$, and $8H_2O/4Ti_{5C}$ configurations are energy optimal and appear gradually on the TiO_2 (101) surface with the surface O_{2C} sites consisting of the O_I–O_{VI} sites (Fig. 6a).

Our DFT calculations revealed that water dissociation is a coverage-dependent process. Increasing the H_2O loading on the Ti_{5C} site of (2 × 2) surface slabs from $1H_2O/1Ti_{5C}$ to $4H_2O/4Ti_{5C}$, the H–O–H bond angle of chemisorbed H_2O is gradually twisted (Fig. 6b), leading to a decline of the dissociation energy of chemisorbed H_2O (Fig. 6c). At the optimal water coverage of $4H_2O$ per TiO_2 (101) (2 × 2) surface slab ($4H_2O/4Ti_{5C}$), water splitting is enhanced, with the dissociation energy dropping to as low as −0.03 eV. This suggests that H_2O dissociation is both exothermic and spontaneous, aligning with our experimental findings. Obviously, the more chemisorbed H_2O on the localized (101) facet of TiO_2, the more favorable to the dissociation of H_2O to form OH. With the further increase of the H_2O loading on the Ti_{5C} site of (2 × 2) surface slabs ($5H_2O/4Ti_{5C}$, $6H_2O/4Ti_{5C}$, and $8H_2O/4Ti_{5C}$), the presence of physisorbed H_2O causes a recovery in the average bond angle of H_2O (Fig. 6b) and an increase in dissociation energy (Fig. 6c), implying that physisorbed H_2O impedes the dissociation of chemisorbed H_2O.

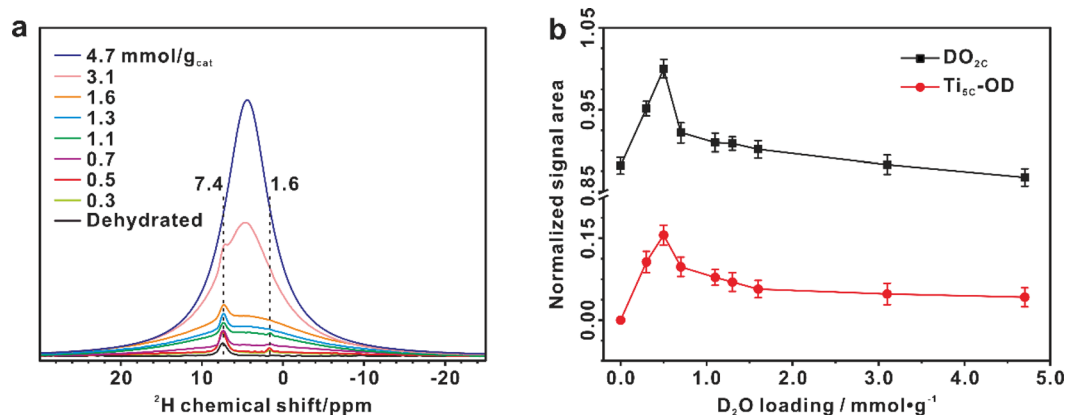To further address the importance of the interplay between OH and H_2O, we also computed the optimized configurations of

Fig. 5 Dissociation of interfacial H_2O validated by 1D ^2H MAS NMR spectra. (a) ^2H MAS NMR spectra of dehydrated ^2H-enriched TiO_2 samples with ^2H_2O loading from 0 to 4.7 mmol g^{-1}. (b) Quantitative evolution of the deuterated bridging OH (DO_{2C}, at 7.4 ppm) and terminal OH (Ti_{5C}-OD, at 1.6 ppm) groups with the increase of H_2O loading, derived from the simulation of the 1D ^2H MAS NMR spectra (Fig. S26†).
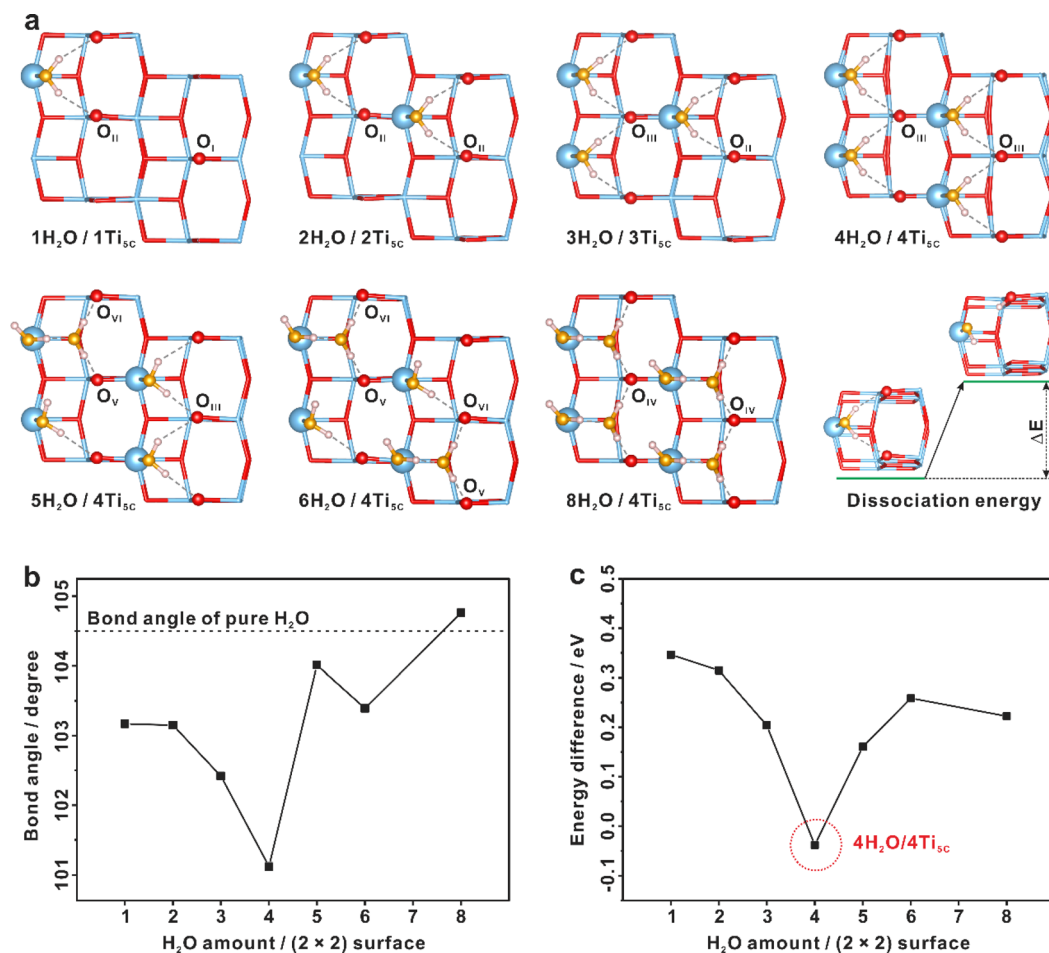
Fig. 6 Dissociation of interfacial H_2O on the TiO_2 surface revealed by DFT calculations. (a) Calculated structures of the TiO_2 (101) (2 × 2) surface slabs with different H_2O adsorption configurations. Titanium and oxygen atoms of TiO_2 are plotted in blue (Ti) and red (O), oxygen atoms originating from the adsorbed H_2O are plotted in yellow (H_2O), and hydrogen atoms are plotted in the pink (H). (b) The average bond angle of interfacial H_2O on the (2 × 2) surface slabs with different H_2O adsorption configurations, calculated from Table S3.† (c) Dissociation energy of interfacial H_2O in the optimized structures of different H_2O adsorption configurations on (2 × 2) TiO_2 (101) surface slabs.
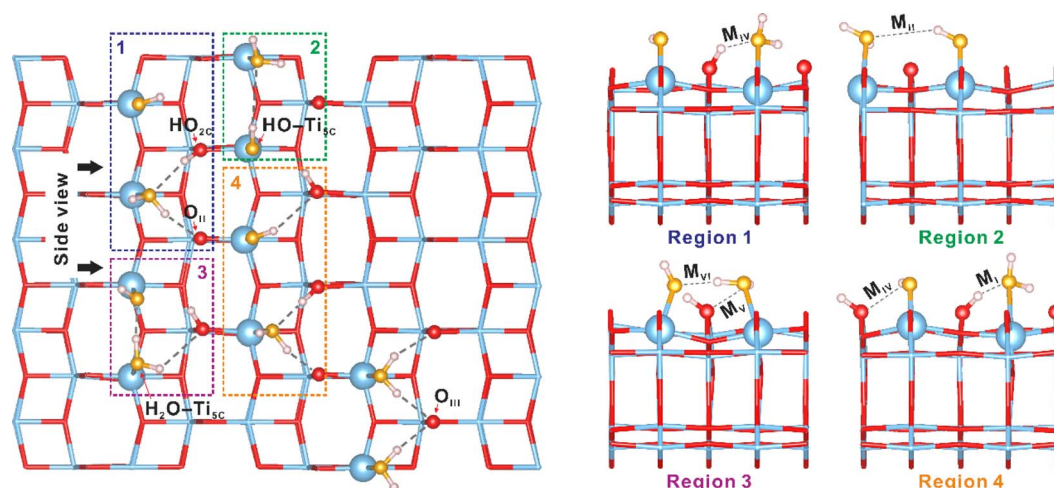

Fig. 7 The role of the OH−H_2O interactions in the dissociation of interfacial H_2O revealed by DFT calculations. The interaction modes of the hydroxyls with chemisorbed H_2O on the (101) facet of TiO_2 at a 40% coverage of water by using a large (5 × 5 × 1) supercell slab with 300 atoms (100 Ti atoms and 200 O atoms), which highlights the optimized atomic structures (M_I–M_{VI}) of hydroxyls and adsorbed H_2O molecules on the surface of TiO_2 shown in Fig. 2c. Regions 1–4 show side views of those structures (M_I–M_{VI}) in the 1–4 regions. Titanium and oxygen atoms of TiO_2 are plotted in blue (Ti) and red (O), oxygen atoms originating from the adsorbed H_2O are plotted in yellow (H_2O), and hydrogen atoms are plotted in pink (H).

the H_2O dissociation state on the (101) facet of TiO_2 at 40% coverage by using a large ($5 \times 5 \times 1$) supercell slab with 300 atoms (100 Ti atoms and 200 O atoms), as presented in Fig. 7 and S27.† It's evident that the OH groups originating from water dissociation have strong interactions with the neighboring chemisorbed H_2O in the M_I–M_{VI} conformations, corroborating with our 2D $^1H\{^{17}O\}$ J-HMQC NMR findings (Fig. 2). This robust interaction stabilizes H_2O dissociation, serving as the driving force for the event. Therefore, at water loadings ranging from 0.3 to 0.5 mmol g^{-1} (approximately 28–46% coverage), massive H_2O dissociation takes place. At elevated water loadings, physisorbed H_2O molecules appear, potentially disrupting the interaction between bridging OH groups (Ti–HO_{2C}–Ti) and chemisorbed H_2O. This promotes the reaction of bridging OH groups with nearby terminal OH groups, leading to the reformation of molecular H_2O (Fig. S28†). All these findings underscore the crucial role of the interplay between OH–H_2O and H_2O–H_2O interactions in determining the behavior of interfacial H_2O on the TiO_2 surface.

Conclusions

In summary, the atomic-level structures and quantitative evolution of surface O/OH sites along with H_2O loading are identified on the TiO_2 (101) surface by solid-state NMR spectroscopy coupled with theoretical calculations. Two types of H_2O (chemisorbed H_2O, i.e. Ti_{5C}–OH_2 and physisorbed H_2O) are present on the H_2O/TiO_2 interface, and detailed interactions between the interfacial H_2O and surface O_{2C}/OH sites are ascertained. We need to mention that the results of the quantitative ^{17}O NMR and ^2H NMR tests have confirmed that, under ambient conditions, a maximum of 41.2% of the total adsorbed H_2O on TiO_2 spontaneously dissociates at a water loading of 0.3 mmol g^{-1}. This means that approximately 0.124 mmol g^{-1} of water dissociates over TiO_2 under these conditions. Our NMR findings and DFT calculations, together with ESR results, confirm that the responsible factor for the observed water rupture at room temperature over the TiO_2 (101) surface is not defects such as oxygen vacancies and impurities, but the joint effect of the coordination-unsaturated Ti_{5C} site and adjacent O_{2C} site, as well as the delicate interplay between water–surface and water–water interactions.

Data availability

The data that support the findings of this study are available within the article and the ESI.†

Author contributions

F. D., N. F., and D. M. conceived the project. N. F. designed the studies. L. Y. synthesized the TiO_2 photocatalysts. N. F., L. Y., J. X., M. W. performed NMR experiments. M. W., Y. J., D. M., L. Y., N. F. and F. D. analyzed all the experimental data. M. H. performed theoretical calculations. N. F., D. M. and F. D. wrote the manuscript. All authors interpreted the data and contributed to the preparation of the manuscript.

Conflicts of interest

The authors declare no competing interests.

Notes and references

1 A. Fujishima and K. Honda, Electrochemical Photolysis of Water at a Semiconductor Electrode, *Nature*, 1972, **238**, 37–38.

2 S. U. M. Khan, M. Al-Shahry and W. B. Ingler, Efficient Photochemical Water Splitting by a Chemically Modified n-TiO_2, *Science*, 2002, **297**, 2243–2245.

3 A. Kudo and Y. Miseki, Heterogeneous photocatalyst materials for water splitting, *Chem. Soc. Rev.*, 2009, **38**, 253–278.

4 Z. Zou, J. Ye, K. Sayama and H. Arakawa, Direct splitting of water under visible light irradiation with an oxide semiconductor photocatalyst, *Nature*, 2001, **414**, 625–627.

5 R. D. Cortright, R. R. Davda and J. A. Dumesic, Hydrogen from catalytic reforming of biomass-derived hydrocarbons in liquid water, *Nature*, 2002, **418**, 964–967.

6 Q. Fu, H. Saltsburg and M. Flytzani-Stephanopoulos, Active Nonmetallic Au and Pt Species on Ceria-Based Water-Gas Shift Catalysts, *Science*, 2003, **301**, 935–938.

7 T. Takata, J. Jiang, Y. Sakata, M. Nakabayashi, N. Shibata, V. Nandal, K. Seki, T. Hisatomi and K. Domen, Photocatalytic water splitting with a quantum efficiency of almost unity, *Nature*, 2020, **581**, 411–414.

8 Z. Liu, E. Huang, I. Orozco, W. Liao, R. M. Palomino, N. Rui, T. Duchon, S. Nemšák, D. C. Grinter, M. Mahapatra, P. Liu, J. A. Rodriguez and S. D. Senanayake, Water-promoted interfacial pathways in methane oxidation to methanol on a CeO_2-Cu_2O catalyst, *Science*, 2020, **368**, 513–517.

9 J. Saavedra, H. A. Doan, C. J. Pursell, L. C. Grabow and B. D. Chandler, The critical role of water at the gold-titania interface in catalytic CO oxidation, *Science*, 2014, **345**, 1599–1602.

10 L. R. Merte, G. Peng, R. Bechstein, F. Rieboldt, C. A. Farberow, L. C. Grabow, W. Kudernatsch, S. Wendt, E. Lægsgaard, M. Mavrikakis and F. Besenbacher, Water-Mediated Proton Hopping on an Iron Oxide Surface, *Science*, 2012, **336**, 889–893.

11 H. Hussain, G. Tocci, T. Woolcot, X. Torrelles, C. L. Pang, D. S. Humphrey, C. M. Yim, D. C. Grinter, G. Cabailh,

O. Bikondoa, R. Lindsay, J. Zegenhagen, A. Michaelides and G. Thornton, Structure of a model TiO_2 photocatalytic interface, *Nat. Mater.*, 2017, **16**, 461–466.

12 O. Björneholm, M. H. Hansen, A. Hodgson, L.-M. Liu, D. T. Limmer, A. Michaelides, P. Pedevilla, J. Rossmeisl, H. Shen, G. Tocci, E. Tyrode, M.-M. Walz, J. Werner and H. Bluhm, Water at Interfaces, *Chem. Rev.*, 2016, **116**, 7698–7726.

13 F. Liu, N. Feng, Q. Wang, J. Xu, G. Qi, C. Wang and F. Deng, Transfer Channel of Photoinduced Holes on a TiO_2 Surface As Revealed by Solid-State Nuclear Magnetic Resonance and Electron Spin Resonance Spectroscopy, *J. Am. Chem. Soc.*, 2017, **139**, 10020–10028.

14 L. Yang, N. Feng, Q. Wang, Y. Chu, J. Xu and F. Deng, Surface Water Loading on Titanium Dioxide Modulates Photocatalytic Water Splitting, *Cell Rep. Phys. Sci.*, 2020, **1**, 100013.

15 Y.-H. Wang, S. Zheng, W.-M. Yang, R.-Y. Zhou, Q.-F. He, P. Radjenovic, J.-C. Dong, S. Li, J. Zheng, Z.-L. Yang, G. Attard, F. Pan, Z.-Q. Tian and J.-F. Li, In situ Raman spectroscopy reveals the structure and dissociation of interfacial water, *Nature*, 2021, **600**, 81–85.

16 S. Nihonyanagi, S. Yamaguchi and T. Tahara, Ultrafast Dynamics at Water Interfaces Studied by Vibrational Sum Frequency Generation Spectroscopy, *Chem. Rev.*, 2017, **117**, 10665–10693.

17 I. V. Stiopkin, C. Weeraman, P. A. Pieniazek, F. Y. Shalhout, J. L. Skinner and A. V. Benderskii, Hydrogen bonding at the water surface revealed by isotopic dilution spectroscopy, *Nature*, 2011, **474**, 192–195.

18 Y. Wang and C. Wöll, IR spectroscopic investigations of chemical and photochemical reactions on metal oxides: bridging the materials gap, *Chem. Soc. Rev.*, 2017, **46**, 1875–1932.

19 J. G. Davis, K. P. Gierszal, P. Wang and D. Ben-Amotz, Water structural transformation at molecular hydrophobic interfaces, *Nature*, 2012, **491**, 582–585.

20 M. G. Walter, E. L. Warren, J. R. McKone, S. W. Boettcher, Q. Mi, E. A. Santori and N. S. Lewis, Solar Water Splitting Cells, *Chem. Rev.*, 2010, **110**, 6446–6473.

21 M. Grätzel, Photoelectrochemical cells, *Nature*, 2001, **414**, 338–344.

22 A. L. Linsebigler, G. Lu and J. T. Yates Jr, Photocatalysis on TiO_2 Surfaces: Principles, Mechanisms, and Selected Results, *Chem. Rev.*, 1995, **95**, 735–758.

23 Y. He, A. Tilocca, O. Dulub, A. Selloni and U. Diebold, Local ordering and electronic signatures of submonolayer water on anatase TiO_2 (101), *Nat. Mater.*, 2009, **8**, 585–589.

24 J. Matthiesen, J. O. Hansen, S. Wendt, E. Lira, R. Schaub, E. Laegsgaard, F. Besenbacher and B. Hammer, Formation and Diffusion of Water Dimers on Rutile TiO_2 (110), *Phys. Rev. Lett.*, 2009, **102**, 226101.

25 J. Carrasco, A. Michaelides, M. Forster, S. Haq, R. Raval and A. Hodgson, A one-dimensional ice structure built from pentagons, *Nat. Mater.*, 2009, **8**, 427–431.

26 K. Onda, B. Li, J. Zhao, K. D. Jordan, J. Yang and H. Petek, Wet Electrons at the H_2O/TiO_2 (110) Surface, *Science*, 2005, **308**, 1154–1158.

27 R. Mu, Z.-j. Zhao, Z. Dohnálek and J. Gong, Structural motifs of water on metal oxide surfaces, *Chem. Soc. Rev.*, 2017, **46**, 1785–1806.

28 Y. Du, N. A. Deskins, Z. Zhang, Z. Dohnálek, M. Dupuis and I. Lyubinetsky, Two Pathways for Water Interaction with Oxygen Adatoms on TiO_2 (110), *Phys. Rev. Lett.*, 2009, **102**, 096102.

29 H. H. Kristoffersen, J. Ø. Hansen, U. Martinez, Y. Y. Wei, J. Matthiesen, R. Streber, R. Bechstein, E. Lægsgaard, F. Besenbacher, B. Hammer and S. Wendt, Role of Steps in the Dissociative Adsorption of Water on Rutile TiO_2 (110), *Phys. Rev. Lett.*, 2013, **110**, 146101.

30 C. Kamal, N. Stenberg, L. E. Walle, D. Ragazzon, A. Borg, P. Uvdal, N. V. Skorodumova, M. Odelius and A. Sandell, Core-Level Binding Energy Reveals Hydrogen Bonding Configurations of Water Adsorbed on TiO_2 (110) Surface, *Phys. Rev. Lett.*, 2021, **126**, 016102.

31 S. Selcuk and A. Selloni, Facet-dependent trapping and dynamics of excess electrons at anatase TiO_2 surfaces and aqueous interfaces, *Nat. Mater.*, 2016, **15**, 1107–1112.

32 W. Yuan, B. Zhu, X.-Y. Li, T. W. Hansen, Y. Ou, K. Fang, H. Yang, Z. Zhang, J. B. Wagner, Y. Gao and Y. Wang, Visualizing H_2O molecules reacting at TiO_2 active sites with transmission electron microscopy, *Science*, 2020, **367**, 428–430.

33 M. A. Henderson, The interaction of water with solid surfaces: fundamental aspects revisited, *Surf. Sci. Rep.*, 2002, **46**, 1–308.

34 U. Diebold, The surface science of titanium dioxide, *Surf. Sci. Rep.*, 2003, **48**, 53–229.

35 C. L. Pang, R. Lindsay and G. Thornton, Structure of Clean and Adsorbate-Covered Single-Crystal Rutile TiO_2 Surfaces, *Chem. Rev.*, 2013, **113**, 3887–3948.

36 Z. Dohnálek, I. Lyubinetsky and R. Rousseau, Thermally-driven processes on rutile TiO_2 (110)-(1 × 1): a direct view at the atomic scale, *Prog. Surf. Sci.*, 2010, **85**, 161–205.

37 A. Vittadini, A. Selloni, F. P. Rotzinger and M. Grätzel, Structure and Energetics of Water Adsorbed at TiO_2 Anatase (101) and (001) Surfaces, *Phys. Rev. Lett.*, 1998, **81**, 2954–2957.

38 A. Tilocca and A. Selloni, Vertical and Lateral Order in Adsorbed Water Layers on Anatase TiO_2 (101), *Langmuir*, 2004, **20**, 8379–8384.

39 M. Sumita, C. Hu and Y. Tateyama, Interface Water on TiO_2 Anatase (101) and (001) Surfaces: First-Principles Study with TiO_2 Slabs Dipped in Bulk Water, *J. Phys. Chem. C*, 2010, **114**, 18529–18537.

40 D. Selli, G. Fazio, G. Seifert and C. Di Valentin, Water Multilayers on TiO_2 (101) Anatase Surface: Assessment of a DFTB-Based Method, *J. Chem. Theory Comput.*, 2017, **13**, 3862–3873.

41 G. S. Herman, Z. Dohnálek, N. Ruzycki and U. Diebold, Experimental Investigation of the Interaction of Water and Methanol with Anatase-TiO2 (101), *J. Phys. Chem. B*, 2003, **107**, 2788–2795.

42 L. E. Walle, A. Borg, E. M. J. Johansson, S. Plogmaker, H. Rensmo, P. Uvdal and A. Sandell, Mixed Dissociative

and Molecular Water Adsorption on Anatase TiO$_2$ (101), *J. Phys. Chem. C*, 2011, **115**, 9545–9550.

43 C. E. Patrick and F. Giustino, Structure of a Water Monolayer on the Anatase TiO$_2$ (101) Surface, *Phys. Rev. A*, 2014, **2**, 014001.

44 M. J. Jackman, A. G. Thomas and C. Muryn, Photoelectron Spectroscopy Study of Stoichiometric and Reduced Anatase TiO$_2$ (101) Surfaces: The Effect of Subsurface Defects on Water Adsorption at Near-Ambient Pressures, *J. Phys. Chem. C*, 2015, **119**, 13682–13690.

45 C. Dette, M. A. Pérez-Osorio, S. Mangel, F. Giustino, S. J. Jung and K. Kern, Single-Molecule Vibrational Spectroscopy of H$_2$O on Anatase TiO$_2$ (101), *J. Phys. Chem. C*, 2017, **121**, 1182–1187.

46 I. M. Nadeem, J. P. W. Treacy, S. Selcuk, X. Torrelles, H. Hussain, A. Wilson, D. C. Grinter, G. Cabailh, O. Bikondoa, C. Nicklin, A. Selloni, J. Zegenhagen, R. Lindsay and G. Thornton, Water Dissociates at the Aqueous Interface with Reduced Anatase TiO$_2$ (101), *J. Phys. Chem. Lett.*, 2018, **9**, 3131–3136.

47 C. Dette, M. A. Pérez-Osorio, S. Mangel, F. Giustino, S. J. Jung and K. Kern, Atomic Structure of Water Monolayer on Anatase TiO$_2$ (101) Surface, *J. Phys. Chem. C*, 2018, **122**, 11954–11960.

48 M. F. Calegari Andrade, H.-Y. Ko, L. Zhang, R. Cara and A. Selloni, Free energy of proton transfer at the water–TiO$_2$ interface from *ab initio* deep potential molecular dynamics, *Chem. Sci.*, 2020, **11**, 2335–2341.

49 F. Fasulo, G. M. Piccini, A. B. Muñoz-García, M. Pavone and M. Parrinello, Dynamics of Water Dissociative Adsorption on TiO$_2$ Anatase (101) at Monolayer Coverage and Below, *J. Phys. Chem. C*, 2022, **126**, 15752–15758.

50 U. Diebold, Perspective: A controversial benchmark system for water-oxide interfaces: H$_2$O/TiO$_2$ (110), *J. Chem. Phys.*, 2017, **147**, 040901.

51 Q. Guo, Z. Ma, C. Zhou, Z. Ren and X. Yang, Single Molecule Photocatalysis on TiO$_2$ Surfaces, *Chem. Rev.*, 2019, **119**, 11020–11041.

52 J. Chen, M. A. Hope, Z. Lin, M. Wang, T. Liu, D. M. Halat, Y. Wen, T. Chen, X. Ke, P. C. M. M. Magusin, W. Ding, X. Xia, X.-P. Wu, X.-Q. Gong, C. P. Grey and L. Peng, Interactions of Oxide Surfaces with Water Revealed with Solid-State NMR Spectroscopy, *J. Am. Chem. Soc.*, 2020, **142**, 11173–11182.

53 S. Schramm and E. Oldfield, High-resolution oxygen-17 NMR of solids, *J. Am. Chem. Soc.*, 1984, **106**, 2502–2506.

54 S. Yang, K. D. Park and E. Oldfield, Oxygen-17 labeling of oxides and zeolites, *J. Am. Chem. Soc.*, 1989, **111**, 7278–7279.

55 T. J. Bastow and S. N. Stuart, ^{17}O NMR in simple oxides, *Chem. Phys.*, 1990, **143**, 459–467.

56 A. V. Chadwick, I. J. F. Poplett, D. T. S. Maitland and M. E. Smith, Oxygen speciation in nanophase MgO from solid-state ^{17}O NMR, *Chem. Mater.*, 1998, **10**, 864–870.

57 N. Kim and C. P. Grey, Probing Oxygen Motion in Disordered Anionic Conductors with ^{17}O and ^{51}V MAS NMR Spectroscopy, *Science*, 2002, **297**, 1317–1320.

58 S. E. Ashbrook and M. E. Smith, Solid state ^{17}O NMR—an introduction to the background principles and applications to inorganic materials, *Chem. Soc. Rev.*, 2006, **35**, 718–735.

59 N. Merle, J. Trebosc, A. Baudouin, I. D. Rosal, L. Maron, K. Szeto, M. Genelot, A. Mortreux, M. Taoufik, L. Delevoye and R. M. Gauvin, ^{17}O NMR gives unprecedented insights into the structure of supported catalysts and their interaction with the silica carrier, *J. Am. Chem. Soc.*, 2012, **134**, 9263–9275.

60 G. P. M. Bignami, D. M. Dawson, V. R. Seymour, P. S. Wheatley, R. E. Morris and S. E. Ashbrook, Synthesis, isotopic enrichment, and solid-state NMR characterization of zeolites derived from the assembly, disassembly, organization, reassembly process, *J. Am. Chem. Soc.*, 2017, **139**, 5140–5148.

61 E. N. Bassey, P. J. Reeves, I. D. Seymour and C. P. Grey, ^{17}O NMR Spectroscopy in Lithium-Ion Battery Cathode Materials: Challenges and Interpretation, *J. Am. Chem. Soc.*, 2022, **144**, 18714–18729.

62 F. Tielens, C. Gervais, G. Deroy, M. Jaber, L. Stievano, C. C. Diogo and J.-F. Lambert, Characterization of Phosphate Species on Hydrated Anatase TiO$_2$ Surfaces, *Langmuir*, 2016, **32**, 997–1008.

63 J. Chen, X.-P. Wu, M. A. Hope, Z. Lin, L. Zhu, Y. Wen, Y. Zhang, T. Qin, J. Wang, T. Liu, X. Xia, D. Wu, X.-Q. Gong, W. Tang, W. Ding, X. Liu, L. Chen, C. P. Grey and L. Peng, Surface differences of oxide nanocrystals determined by geometry and exogenously coordinated water molecules, *Chem. Sci.*, 2022, **13**, 11083.

64 M. Wang, X.-P. Wu, S. Zheng, L. Zhao, L. Li, L. Shen, Y. Gao, N. Xue, X. Guo, W. Huang, Z. Gan, F. Blanc, Z. Yu, X. Ke, W. Ding, X.-Q. Gong, C. P. Grey and L. Peng, Identification of Different Oxygen Species in Oxide Nanostructures with ^{17}O Solid-State NMR Spectroscopy, *Sci. Adv.*, 2015, **1**, e1400133.

65 Y. Li, X.-P. Wu, N. Jiang, M. Lin, L. Shen, H. Sun, Y. Wang, M. Wang, X. Ke, Z. Yu, F. Gao, L. Dong, X. Guo, W. Hou, W. Ding, X.-Q. Gong, C. P. Grey and L. Peng, Distinguishing Faceted Oxide Nanocrystals with ^{17}O Solid-State NMR Spectroscopy, *Nat. Commun.*, 2017, **8**, 581.

66 B. Song, Y. Li, X.-P. Wu, F. Wang, M. Lin, Y. Sun, A.-P. Jia, X. Ning, L. Jin, X. Ke, Z. Yu, G. Yang, W. Hou, W. Ding, X.-Q. Gong and L. Peng, Unveiling the Surface Structure of ZnO Nanorods and H$_2$ Activation Mechanisms with ^{17}O NMR Spectroscopy, *J. Am. Chem. Soc.*, 2022, **144**, 23340–23351.

67 Q. Wang, W. Li, I. Hung, F. Mentink-Vigier, X. Wang, G. Qi, X. Wang, Z. Gan, J. Xu and F. Deng, Mapping the oxygen structure of γ-Al$_2$O$_3$ by high-field solid-state NMR spectroscopy, *Nat. Commun.*, 2020, **11**, 3620.

68 L. Liu, X. Gu, Z. Ji, W. Zou, C. Tang, F. Gao and L. Dong, Anion-Assisted Synthesis of TiO$_2$ Nanocrystals with Tunable Crystal Forms and Crystal Facets and Their Photocatalytic Redox Activities in Organic Reactions, *J. Phys. Chem. C*, 2013, **117**, 18578–18587.

69 A. Jia, Y. Zhang, T. Song, Z. Zhang, C. Tang, Y. Hu, W. Zheng, M. Luo, J. Lu and W. Huang, Crystal-plane effects of anatase TiO$_2$ on the selective hydrogenation of crotonaldehyde over Ir/TiO$_2$ catalysts, *J. Catal.*, 2021, **395**, 10–22.